

# Age classes stratified by risk and adaptive behavior during epidemics

Ronan F. Arthur,  
School of Medicine  
Stanford University

May Levin  
Department of Biology  
Stanford University

Alexandre Labrogere  
Department of Management Science & Engineering  
Stanford University

Marcus W. Feldman  
Department of Biology  
Stanford University

May 26, 2023

## Abstract

Heterogeneity in contact patterns, mortality rates, and transmissibility among and between different age classes can have significant effects on epidemic outcomes. Adaptive behavior in response to the spread of an infectious pathogen may give rise to complex epidemiological dynamics. Here we model an infectious disease in which adaptive behavior incentives, and mortality rates, can vary between three age classes. The model indicates that age-dependent variability in infection aversion can produce more complex epidemic dynamics at lower levels of pathogen transmissibility.

## 1 Introduction

One of the principal failings of the attempts to model and predict future trends and dynamics of infectious disease epidemics has been the lack of incorporation of human behavior into these models [1]. The social drivers of infectious disease dynamics have been relatively neglected in the academic literature compared with the vast resources and attention paid to the biomedical and, to a lesser extent, the ecological drivers of disease [2,3]. COVID-19, however, has shone a spotlight on this discrepancy as socio-cultural factors have played an important role in the pandemic – from the political polarization of risk perception in the United States [4] to the social, cultural, and demographic factors associated with vaccine hesitancy [5]. Models should incorporate relevant social phenomena, as well as their interactions, as the study of each phenomenon in isolation may not be informative or useful.

24 For example, adaptive age-specific preventative behaviors motivated by differentiated risk  
25 of COVID-19 mortality should be included. The resulting contact patterns and associated  
26 infection dynamics are expected to interact in their influence on epidemic trajectories.

27 The mortality rate of COVID-19 is highly age-specific [6] with a log-linear increase of  
28 infection fatality ratio by age among individuals over 30 [7]. This contributes to skewed  
29 risk perceptions across the population's age structure and economic activity associated with  
30 COVID-19 risk [8,9]. Heterogeneity in contact patterns, mortality rates, and transmissibility  
31 among and between different age classes is known to have significant effects on epidemic  
32 outcomes [10,11]. In Germany, for example, younger adults and teenagers were likely the  
33 main drivers of COVID-19 transmission dynamics during the first three pandemic waves [12].  
34 Goldstein et al. [13] found that vaccinating the elderly first against COVID-19 would save  
35 the most lives, although the model neglected key features of transmission dynamics [14].  
36 Further, Acemoglu and colleagues showed that optimal lockdown policies during COVID-  
37 19 are age-specific, with strict lockdown policies on the oldest group and reduction of  
38 interactions between age classes being most effective [15]. Their model, however, assumed  
39 exogenous targeted policies and did not incorporate adaptive behavior, a cornerstone of  
40 COVID-19 dynamics.

41 As risk of transmission of a dangerous infection increases during an epidemic, individuals  
42 and governments tend to react by mitigating that risk with adaptive behavior. Adaptive  
43 behavior has enjoyed growing attention in the disease modeling literature [16,17], with  
44 techniques using game theory [18], fear-infection parallel contagions [19,20], and network-  
45 and agent-based approaches [21]. Early work by Capasso et al. [22] experimented with  
46 the introduction of a negative feedback mechanism in the traditional susceptible-infected-  
47 recovered (SIR) model [23] and represented reduced contacts as a function of the number  
48 of infected. Philipson formalized the economic theory of adaptive behavior showing that  
49 rational agents following dynamic incentives may lead to oscillations around an indifference  
50 point, or equilibrium [24]. Adaptive behavior can cause oscillatory dynamics because a  
51 system with a negative feedback can continuously overshoot adjustments [25,26].

52 Adaptive behavior may also lead to complex dynamics that are characteristic of determin-  
53 istic, chaotic systems, especially with delays in adaptive response [27]. Empirical evidence  
54 from the COVID-19 pandemic suggests that the behavior of the epidemic has been chaotic  
55 in a majority of countries [28]. An investigation of the second derivative of infections over  
56 time during COVID-19 found that the pandemic qualitatively met Henri Poincaré's criteria  
57 for chaos in deterministic dynamical systems: a large number of solutions, dynamic sensi-  
58 tivity, and numerical unpredictability [29]. Measles models show characteristically chaotic  
59 dynamics that may also characterize the observed dynamics [30,31]. In the SEIR framework

60 with a periodically varying contact rate that represented seasonal changes, sustained oscillations [32] and period-doubling bifurcations [33] were found, and one case with a particularly  
61 high degree of contact led to chaotic dynamics [34]. While age structure heterogeneity in  
62 susceptibility and seasonal variance in contact rates due to school attendance characterize  
63 measles modeling [35, 36], age structure heterogeneity in dynamic, adaptive contact rates  
64 have not been modeled for COVID-19.

66 Here, we model an infectious disease with adaptive behavior incentives of the form used in a  
67 previous model [27] and include different mortality rates for three age classes: the “young,”  
68 the “middle-aged,” and the “old” (à la Acemoglu et al. [15]).

## 69 2 Model specifications

70 We begin with a susceptible-infected-susceptible (SIS) compartmental disease model [37],  
71 which includes an adaptive contact behavior that maximizes a utility function, as in Arthur  
72 et al. [27]. With susceptible and infectious individuals, denoted by  $S_t$  and  $I_t$ , respectively,  
73 at time  $t$ , and  $N_t$  the population size, we have:

$$S_{t+1} = S_t - b_0 c_t^* S_t I_t + \gamma I_t \quad (2.1)$$

$$I_{t+1} = I_t + b_0 c_t^* S_t I_t - \gamma I_t \quad (2.2)$$

$$S_t + I_t = N_t, \quad (2.3)$$

74 where  $b_0$  represents transmissibility given contact,  $\gamma$  represents the removal rate, and  $c_t^*$   
75 represents a contact rate at time  $t$  chosen to maximize utility  $U(c)$  as a function of contacts:

$$U(c) = \alpha_0 - \alpha_1 (c - \hat{c})^2 - \alpha_2 \left\{ 1 - \left[ 1 - \left( \frac{I_{t-\Delta}}{N} \right) b_0 \right]^c \right\}. \quad (2.4)$$

76 Here,  $c$  represents contacts per unit time,  $\hat{c}$  represents the optimal contact rate when the  
77 disease risk is non-existent,  $\alpha_1$  represents the utility gained by achieving  $\hat{c}$  contacts and  $\alpha_2$   
78 represents the utility lost if infected. Here,  $\Delta$  represents delayed information, such that  
79 an individual may base their perception of infection risk on prevalence during past time  
80 periods, rather than the current one. Maximizing Eq 2.4 with respect to  $c$  yields  $c_t^*$ , the  
81 contact rate chosen at each time step to maximize utility.

82 To incorporate age structure, we stratify the population into  $k$  discrete age classes, repre-  
 83 sented by  $A_1, \dots, A_k$ . The number in sub-population  $A_i$  is given by  $N_i$ . We assume the  
 84 size of each age class does not change:  $N_{it} = N_i$  and let  $\sum_{i=1}^k N_i = N$ . The utility function  
 85 (as in Eq 2.4) for each age class  $i$  is given by

$$U_i(c) = \alpha_0 - \alpha_{1i}(c - \hat{c}_i)^2 - \alpha_{2i} \left\{ 1 - \left[ 1 - \left( \frac{I_{t-\Delta}}{N} \right) b_0 \right]^c \right\}, \quad (2.5)$$

86 where  $\alpha_{1i}$  represents the utility loss of reduced contacts for  $A_i$ ,  $\hat{c}_i$  represents the target  
 87 contact rate for  $A_i$ , and  $\alpha_{2i}$  represents the utility loss (i.e. aversion) to infection based on  
 88 a delayed perception of population-level prevalence for  $A_i$ . Here it is assumed that each  
 89 age class perceives its risk according to the disease prevalence of the whole population (i.e.  
 90  $I_{t-\Delta} = \sum_{i=1}^k I_{i,t-\Delta}$ ), rather than just of their own group.

91 Interactions between and within age classes at time  $t$  are defined in terms of a dynamic  
 92 contact matrix  $M_t$  (censu Ram & Schaposnik, 2021 [38]),

$$M_t = \begin{bmatrix} c_{1t}^* & c_{12} & \dots & c_{1k} \\ c_{21} & c_{2t}^* & \dots & c_{2k} \\ \vdots & \vdots & \ddots & \vdots \\ c_{k1} & c_{k2} & \dots & c_{kt}^* \end{bmatrix}, \quad (2.6)$$

93 where  $c_{it}^*$  represents the within-group contact of  $A_i$ , optimized at time step  $t$  to maximize  
 94 utility in  $A_i$  (as in Eq 2.4), and  $c_{ij}$  represents the contact between  $A_i$  and  $A_j$  for  $i \neq j$ . For  
 95 simplicity, institutional behavior change is assumed to only affect the within-group contact  
 96 (e.g., via school and workplace closures and nursing home quarantines), and thus, between-  
 97 group contact rates are assumed fixed and not adaptive to changing infection risks. It is  
 98 assumed that  $c_{ij} = c_{ji}$ .

99 Using the contact matrix (2.6), the transition between susceptible and infected disease states  
 100 for age class  $A_i$ , as in Eqs. 2.1-2.3, can be expressed as

$$S_{i(t+1)} = S_{it} - b_0 c_{it}^* S_{it} I_{it} - \sum_{j=1, i \neq j}^k b_0 c_{ij} S_{it} I_{jt} + \gamma_i I_{it}, \quad (2.7)$$

$$I_{i(t+1)} = I_{it} + b_0 c_{it}^* S_{it} I_{it} + \sum_{j=1, i \neq j}^k b_0 c_{ij} S_{it} I_{jt} - \gamma_i I_{it}, \quad (2.8)$$

$$S_{it} + I_{it} = N_{it}. \quad (2.9)$$

101 We assume the following constraints:

102 1. The aversion to infection is greatest in the elderly and least in the young, i.e.,

$$\alpha_{2k} > \cdots > \alpha_{21}. \quad (2.10)$$

103 2. The target contact rate is greatest in the young and least in the elderly, i.e.,

$$\hat{c}_1 > \cdots > \hat{c}_k. \quad (2.11)$$

104 3. The recovery rate from the infected category to the susceptible is the same for all age  
105 classes, namely, for all  $i, j$ ,

$$\gamma_i = \gamma_j = \gamma. \quad (2.12)$$

106 4. The number of infecteds in any age class  $A_i$  may never be greater than the population  
107 size of that class or less than zero, i.e. for all  $i$  and  $t$ ,

$$0 \leq I_{it} \leq N_i. \quad (2.13)$$

## 108 3 Analytical Results

### 109 3.1 Equilibria

110 To understand the dynamic behavior of the number of infecteds in each age class, we first  
111 examine conditions for the existence of equilibria. If  $I_t b_0$  is small relative to  $N$ , then on  
112 linearizing with respect to  $I$  in Eq 2.5, the optimal value of  $c_i$  at time  $t$  for  $A_i$  is found to be

$$c_{it}^* = \hat{c}_i - \frac{\alpha_{2i} b_0 I_{t-\Delta}}{2\alpha_{1i} N}. \quad (3.1)$$

113 Define the parameter  $\alpha_i$  as

$$\alpha_i = \frac{\alpha_{2i} b_0}{2\alpha_{1i}}. \quad (3.2)$$

114 We begin with a 2-age-class model, where  $A_1$  represents the youth and  $A_2$  represents the  
115 middle-aged and elderly, in which case, Eqs. 2.6-2.13, with  $k = 2$ , become

$$M_t = \begin{bmatrix} c_{1t}^* & c_{12} \\ c_{12} & c_{2t}^* \end{bmatrix}, \quad (3.3)$$

$$I_{1(t+1)} = I_{1t} + b_0 c_{1t}^* S_{1t} I_{1t} + b_0 c_{12} S_{1t} I_{2t} - \gamma I_{1t}, \quad (3.4)$$

116  $I_{2(t+1)} = I_{2t} + b_0 c_{2t}^* S_{2t} I_{2t} + b_0 c_{12} S_{2t} I_{1t} - \gamma I_{2t}, \quad (3.5)$

117 with  $S_{1t} + I_{1t} = N_1$ ,  $S_{2t} + I_{2t} = N_2$ , and  $N = N_1 + N_2$ .

118 For simplicity, we assume the population sizes of all groups are equal (i.e.  $N_1 = N_2 = \frac{N}{2}$ ).

119 Then, substituting  $c_{1t}^*$  from Eq 3.1 and  $\alpha_1$  from Eq 3.2, with  $\Delta = 0$ , we obtain

$$I_{1(t+1)} = I_{1t} - \gamma I_{1t} + b_0[\hat{c}_1 - \alpha_1 \frac{(I_{1t} + I_{2t})}{N}](\frac{N}{2} - I_{1t})I_{1t} + b_0 c_{12} I_{2t}(\frac{N}{2} - I_{1t}). \quad (3.6)$$

$$= f_1(I_{1t}, I_{2t}) \quad (3.7)$$

$$= \frac{\alpha_1 b_0}{N} I_{1t}^3 + (\alpha_1 b_0 \frac{I_{2t}}{N} - b_0 \hat{c}_1 - \frac{\alpha_1 b_0}{2}) I_{1t}^2 + (b_0 \hat{c}_1 \frac{N}{2} - \frac{b_0 \alpha_1 I_{2t}}{2} - b_0 c_{12} I_{2t} + 1 - \gamma) I_{1t} + b_0 c_{12} I_{2t} \frac{N}{2}. \quad (3.8)$$

120 By symmetry,

$$I_{2(t+1)} = \frac{\alpha_2 b_0}{N} I_{2t}^3 + (\alpha_2 b_0 \frac{I_{1t}}{N} - b_0 \hat{c}_2 - \frac{\alpha_2 b_0}{2}) I_{2t}^2 + (b_0 \hat{c}_2 \frac{N}{2} - \frac{b_0 \alpha_2 I_{1t}}{2} - b_0 c_{12} I_{1t} + 1 - \gamma) I_{2t} + b_0 c_{12} I_{1t} \frac{N}{2}. \quad (3.9)$$

$$= f_2(I_{1t}, I_{2t}). \quad (3.10)$$

122 A fixed point (i.e., equilibrium) exists for  $A_i$  when  $I_{i(t+1)} = I_{it}$  for  $i = 1, 2$ . Thus, equilibria  
123 are the roots of the two simultaneous polynomial equations

$$0 = \frac{\alpha_1 b_0}{N} I_1^3 + (\alpha_1 b_0 \frac{I_2}{N} - b_0 \hat{c}_1 - \frac{\alpha_1 b_0}{2}) I_1^2 + (b_0 \hat{c}_1 \frac{N}{2} - \frac{b_0 \alpha_1 I_2}{2} - b_0 c_{12} I_2 - \gamma) I_1 + b_0 c_{12} I_2 \frac{N}{2} \quad (3.11)$$

124 and

$$0 = \frac{\alpha_2 b_0}{N} I_2^3 + (\alpha_2 b_0 \frac{I_1}{N} - b_0 \hat{c}_2 - \frac{\alpha_2 b_0}{2}) I_2^2 + (b_0 \hat{c}_2 \frac{N}{2} - \frac{b_0 \alpha_2 I_1}{2} - b_0 c_{12} I_1 - \gamma) I_2 + b_0 c_{12} I_1 \frac{N}{2} \quad (3.12)$$

### 125 3.2 Stability

126 To analyze local stability, we calculate the Jacobian of the differential equations corre-  
127 sponding to Eqs 3.8-3.9, where  $I_{1(t+1)} = f_1(I_{1t}, I_{2t})$  and  $I_{2(t+1)} = f_2(I_{1t}, I_{2t})$  and evaluate  
128 the Jacobian at the equilibrium. Differentiating each function with respect to each variable  
129  $I_1$  and  $I_2$ ,

$$\frac{\partial f_1}{\partial I_1} = 3\frac{\alpha_1 b_0}{N} I_1^2 + 2(\alpha_1 b_0 \frac{I_2}{N} - b_0 \hat{c}_1 - \alpha_1 b_0 \frac{N_1}{N}) I_1 + (b_0 \hat{c}_1 N_1 - b_0 \alpha_1 I_2 \frac{N_1}{N} - b_0 c_{12} I_2 + 1 - \gamma), \quad (3.13)$$

$$\frac{\partial f_1}{\partial I_2} = \frac{b_0 \alpha_1}{N} I_1^2 - b_0 \alpha_1 \frac{N_1}{N} I_1 - b_0 c_{12} I_1 + b_0 c_{12} N_1, \quad (3.14)$$

$$\frac{\partial f_2}{\partial I_1} = \frac{b_0 \alpha_2}{N} I_2^2 - b_0 \alpha_2 \frac{N_2}{N} I_2 - b_0 c_{12} I_2 + b_0 c_{12} N_2, \quad (3.15)$$

$$\frac{\partial f_2}{\partial I_2} = 3\frac{\alpha_2 b_0}{N} I_2^2 + 2(\alpha_2 b_0 \frac{I_1}{N} - b_0 \hat{c}_2 - \alpha_2 b_0 \frac{N_2}{N}) I_2 + (b_0 \hat{c}_2 N_2 - b_0 \alpha_2 I_1 \frac{N_2}{N} - b_0 c_{12} I_1 + 1 - \gamma). \quad (3.16)$$

## 130 4 Computational Results

### 131 4.1 The 2-population model

132 We first examine the numerical iteration of the discrete time SIS recursions (Eqs 3.8-3.9)  
133 without time-delay, and set default values for all parameters, namely:

134  $N_1 = 5000$ ,  $N_2 = 5000$ ,  $I_0 = 1$ ,  $\gamma_1 = 0.1$ ,  $\gamma_2 = 0.1$ ,  $\hat{c}_1 = 0.02$ ,  $\hat{c}_2 = 0.01$ ,  $c_{12} = 0.005$ ,  $\alpha_1 = 1$ ,  
135  $\alpha_{21} = 20$ ,  $\alpha_{22} = 40$ ,  $b_0 = 0.009$ .

136 By increasing the transmissibility parameter  $b_0$  from the default value, we see a progression  
137 of dynamical regimes across critical thresholds from simple convergence to cyclic behavior  
138 in 2, 4, and 6-point cycles, chaos, and collapse (Figs 1,3,5). By increasing the contact rate  
139 between the 2 populations,  $c_{12}$ , there is a progression from simple convergence to a 2-pt  
140 cycle, 6-pt cycle, chaos, back to a 6-pt cycle, and finally an asynchronous 8-pt and 2-pt  
141 cycle (Figs 2,4).

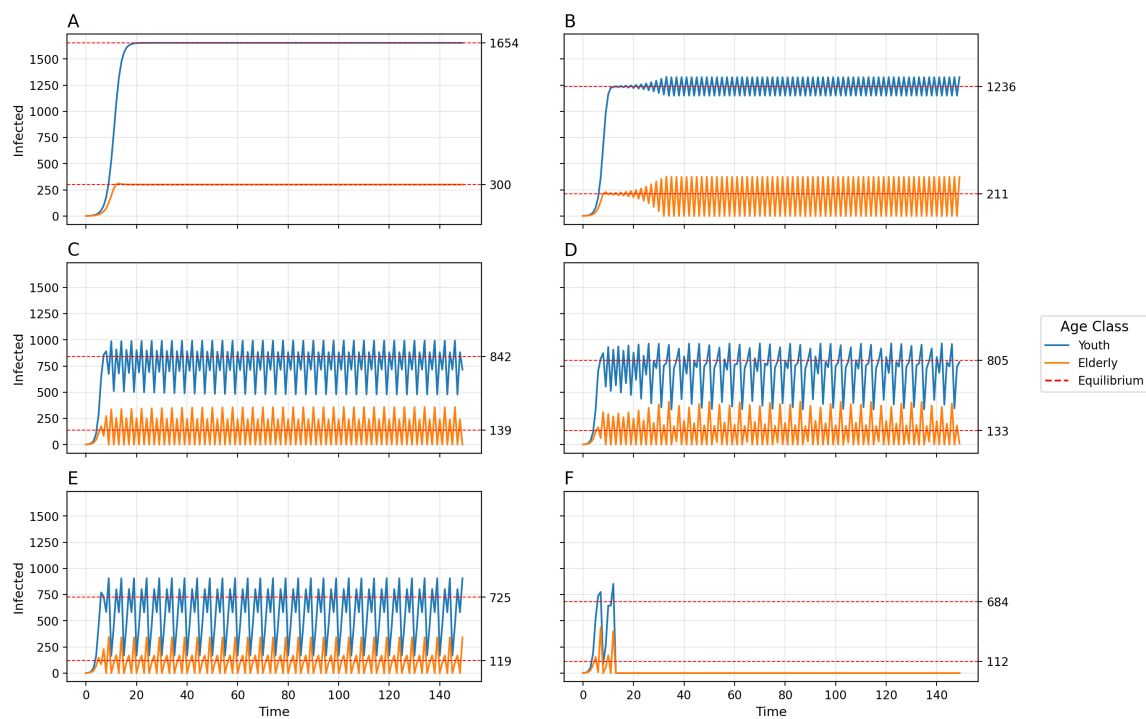


Figure 1: Disease dynamics for 2-population age-structured model using default parameters and varying transmissibility  $b_0$ . A)  $b_0 = 0.009$ , Convergence to stable equilibria; B)  $b_0 = 0.013$ , 2-point cycle; C)  $b_0 = 0.02$ , 4-point cycle; D)  $b_0 = 0.021$ , chaos; E)  $b_0 = 0.0235$ , 6-pt cycle; F)  $b_0 = 0.025$ , Collapse.



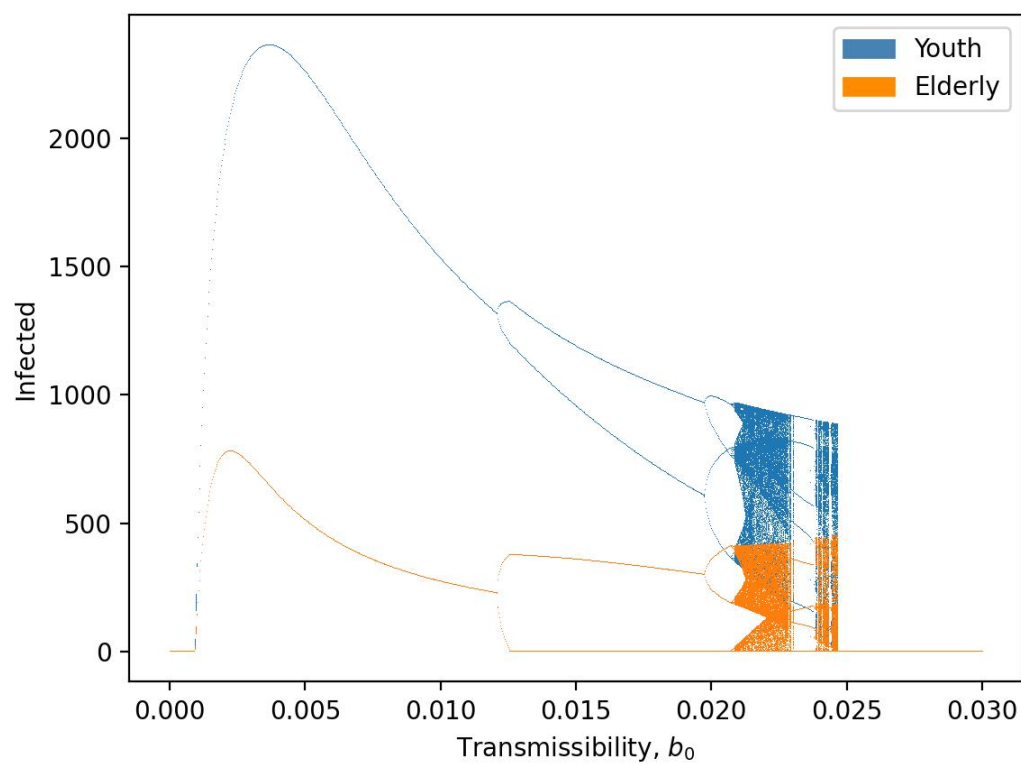


Figure 2: Bifurcation diagram of equilibria, oscillatory dynamics, and chaotic behavior as a function of transmissibility  $b_0$ .

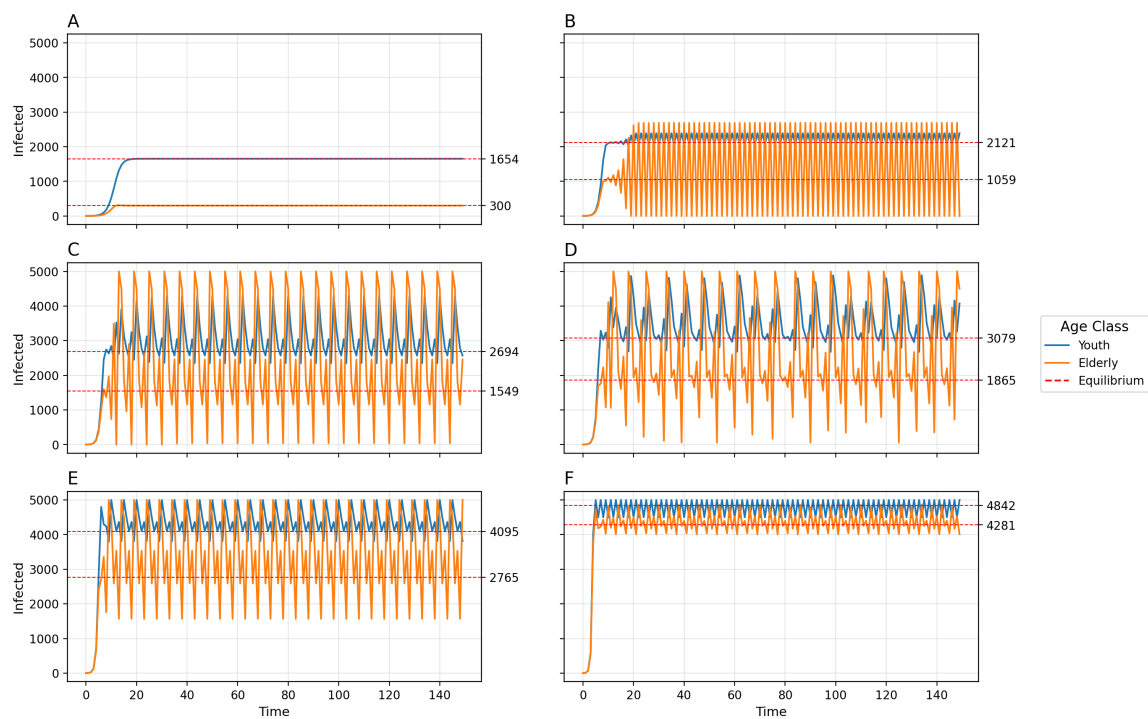


Figure 3:

Disease dynamics for 2-population age-structured model using default parameters and varying between-group contact rate  $c_{12}$ . A)  $c_{12} = 0.005$ , Convergence to stable equilibria; B)  $c_{12} = 0.025$ , 2-point cycle; C)  $c_{12} = 0.04$ , 6-point cycle; D)  $c_{12} = 0.05$ , chaos; E)  $c_{12} = 0.08$ , 6-pt cycle; F)  $c_{12} = 0.15$ , 8-pt cycle for Old and 2-pt cycle for Young.

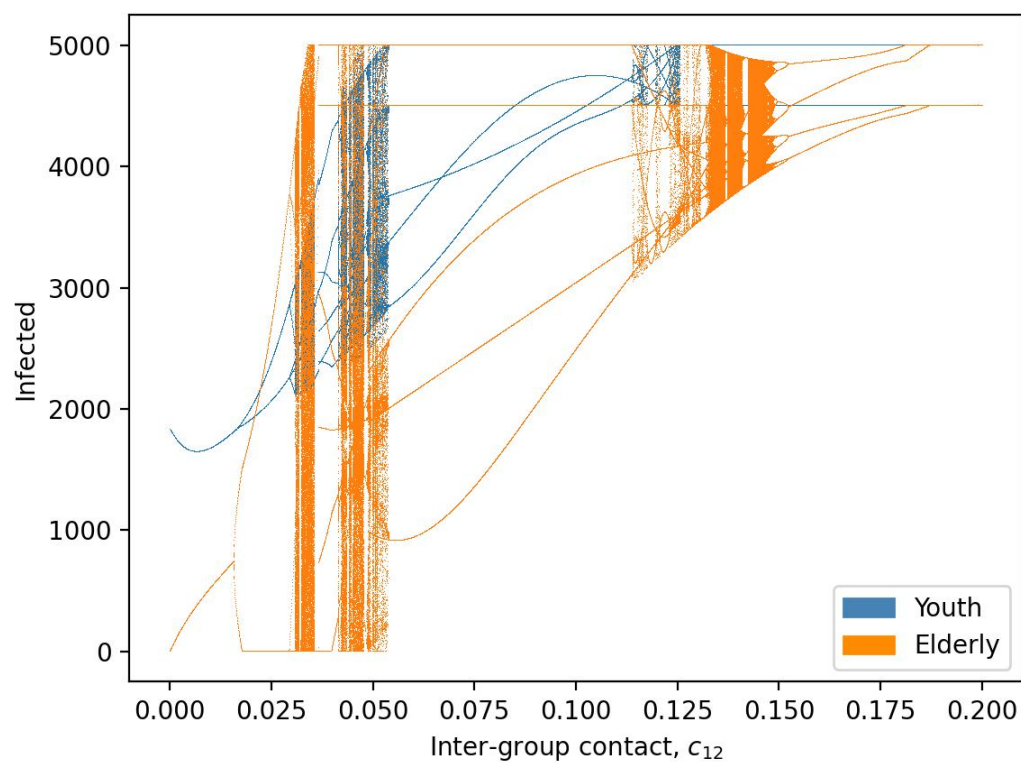


Figure 4:  
Bifurcation diagram of equilibria, oscillatory dynamics, and chaotic behavior as a function of inter-group contact rate  $c_{12}$ .

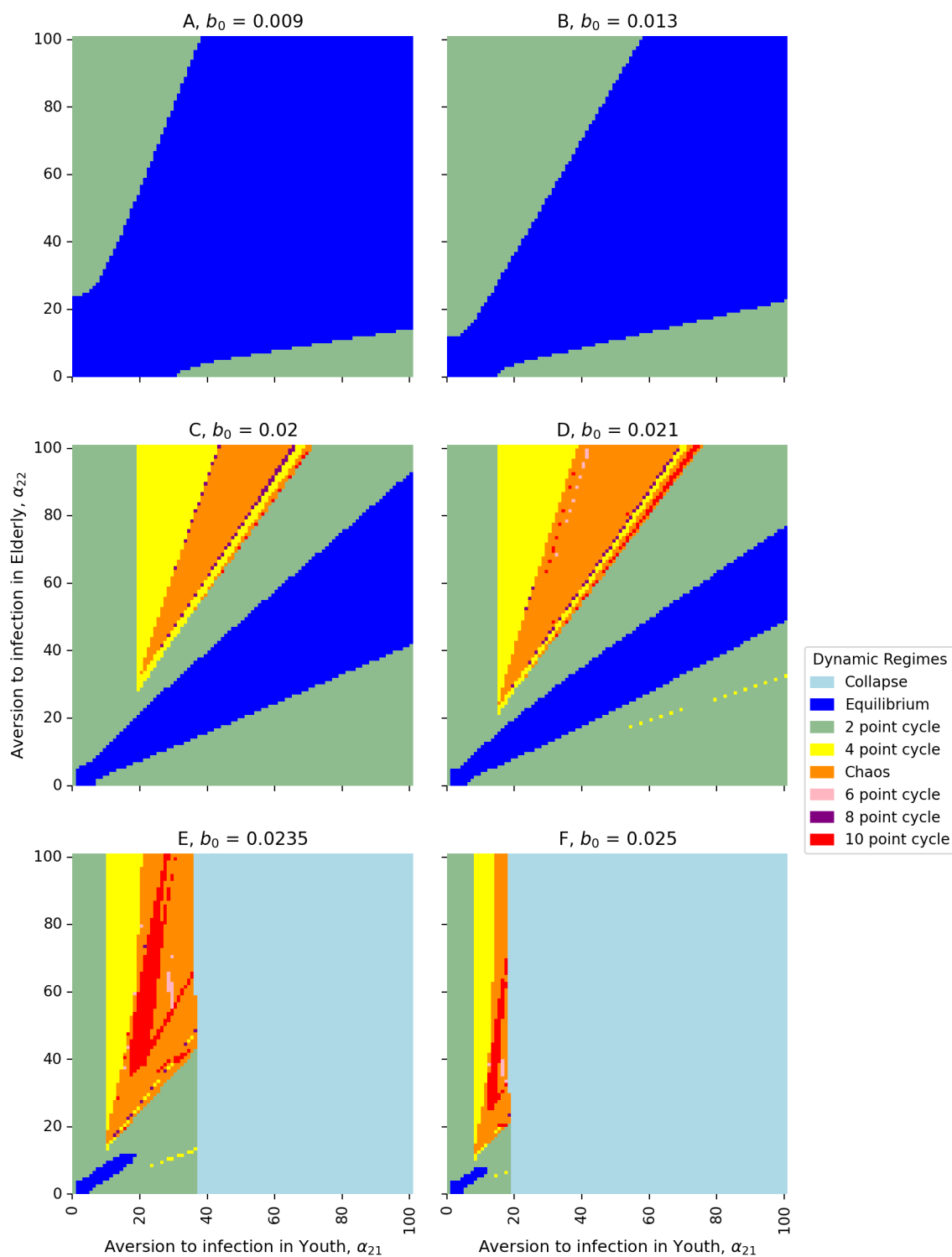


Figure 5:

Heat maps of dynamic regimes as a function of the relationship between aversion to infection in the youth ( $\alpha_{21}$ ) and in the elderly ( $\alpha_{22}$ ) with varying transmissibility ( $b_0$ ): A)  $b_0 = 0.009$ ; B)  $b_0 = 0.013$ ; C)  $b_0 = 0.02$ ; D)  $b_0 = 0.021$ ; E)  $b_0 = 0.0235$ ; F)  $b_0 = 0.025$ .

## 142 4.2 The 3-population model

143 For our 3-age-class model,  $A_1$  represents the youth,  $A_2$  represents the middle-aged, and  $A_3$   
144 represents the elderly. Then the analogous equations to Eqs 2.6-2.13, for  $k = 3$ , are

$$M_t = \begin{bmatrix} c_{t1}^* & c_{12} & c_{13} \\ c_{12} & c_{t2}^* & c_{23} \\ c_{13} & c_{23} & c_{t3}^* \end{bmatrix}, \quad (4.1)$$

$$145 \quad I_{1(t+1)} = I_{1t} + b_0 c_{1t}^* S_{1t} I_{1t} + b_0 c_{12} S_{1t} I_{2t} + b_0 c_{13} S_{1t} I_{3t} - \gamma I_{1t}, \quad (4.2)$$

$$146 \quad I_{2(t+1)} = I_{2t} + b_0 c_{2t}^* S_{2t} I_{2t} + b_0 c_{12} S_{2t} I_{1t} + b_0 c_{23} S_{2t} I_{3t} - \gamma I_{2t}, \quad (4.3)$$

$$I_{3(t+1)} = I_{3t} + b_0 c_{3t}^* S_{3t} I_{3t} + b_0 c_{13} S_{3t} I_{1t} + b_0 c_{23} S_{3t} I_{2t} - \gamma I_{3t}, \quad (4.4)$$

147 with

$$S_{1t} + I_{1t} = N_1, S_{2t} + I_{2t} = N_2, S_{3t} + I_{3t} = N_3. \quad (4.5)$$

148 Equilibria for the system defined by Eqs. 4.2-4.4 solve  $I_{i(t+1)} = I_{it}$  for  $i = [1, 2, 3]$  and are  
149 the roots of three simultaneous polynomial equations.

150 We set default values for parameters and initial conditions, such that

$$151 \quad N_1 = 5000, N_2 = 5000, N_3 = 5000, I_0 = 1, \gamma_1 = 0.1, \gamma_2 = 0.1, \gamma_3 = 0.1, \hat{c}_1 = 0.02,$$
$$152 \quad \hat{c}_2 = 0.015, \hat{c}_3 = 0.01, c_{12} = 0.005, c_{13} = 0.003, c_{23} = 0.007, \alpha_1 = 1, \alpha_{21} = 20, \alpha_{22} = 30,$$
$$153 \quad \alpha_{23} = 40, b_0 = 0.01.$$

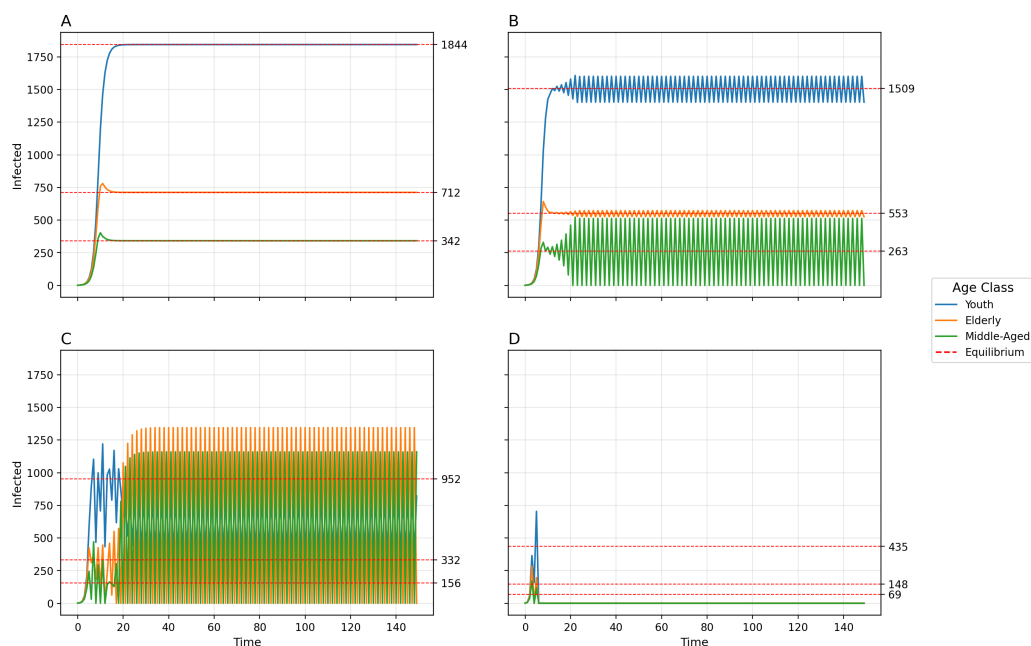


Figure 6: Disease dynamics for 3-population age-structured model using default parameters and varying transmissibility  $b_0$ . A)  $b_0 = 0.01$ , Convergence to stable equilibria; B)  $b_0 = 0.013$ , 2-point cycle; C)  $b_0 = 0.022$ , Chaos into a 2-pt cycle cycle; D)  $b_0 = 0.05$ , Collapse.

154 By increasing the transmissibility  $b_0$ , the model goes from simple convergence to a 2-point  
 155 cycle to chaos into a 2-pt cycle to collapse (Fig 6). By uniformly increasing the between-  
 156 group contact rates  $c_{12}$ ,  $c_{13}$ , and  $c_{23}$ , the model exhibits convergence, a 2-pt cycle, a 4-pt  
 157 cycle, chaos, a 5-py cycle, and a 6-pt cycle. The amplitude of oscillations and the variance of  
 158 chaotic dynamics are greatest for the elderly population and least for the youth population.

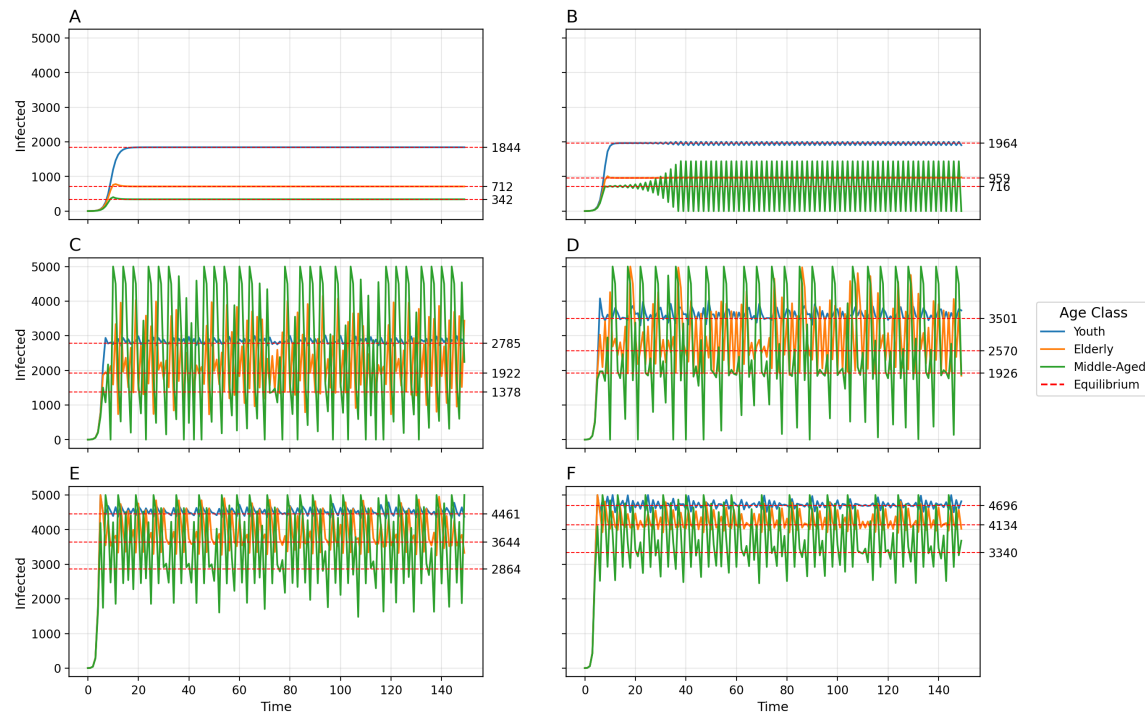


Figure 7:

Disease dynamics for 3-population age-structured model using default parameters and varying between-group contact rates  $c_{12}$ ,  $c_{13}$ , and  $c_{23}$ .

- A)  $c_{12} = 0.005$ ,  $c_{13} = 0.003$ ,  $c_{23} = 0.007$ , Convergence to stable equilibria; B)  $c_{12} = 0.008$ ,  $c_{13} = 0.01$ ,  $c_{23} = 0.01$ , 2-point cycle; C)  $c_{12} = 0.022$ ,  $c_{13} = 0.02$ ,  $c_{23} = 0.024$ , 4-point cycle; D)  $c_{12} = 0.032$ ,  $c_{13} = 0.03$ ,  $c_{23} = 0.034$ , Chaos; E)  $c_{12} = 0.05$ ,  $c_{13} = 0.048$ ,  $c_{23} = 0.052$ , 5-pt cycle; F)  $c_{12} = 0.06$ ,  $c_{13} = 0.058$ ,  $c_{23} = 0.062$ , 6-pt cycle.

## 159 5 Discussion

160 Results from the 2- and 3-population adaptive behavior models indicate that, for certain  
 161 parameter values, stable equilibria can be reached for each sub-population  $i$ , including 0  
 162 for all age groups and an equilibrium between 0 and  $N_i$ . In the 2-population case, the  
 163 equilibrium for each population can be derived numerically. With increasing values of  $b_0$   
 164 and  $c_{ij}$  (the transmissibility and between-group contact rate, respectively), the system may  
 165 converge to a non-zero equilibrium, oscillate perpetually with 2-, 4-, 6-, 8-, and 10-period  
 166 intervals, become chaotic, and collapse. Complexity of dynamics can be found at lower  
 167 levels of transmissibility with greater differentiation between aversions to infection (Fig 5).  
 168 For both the 2-population and 3-population models, the younger population has a higher

169 non-zero equilibrium size than the older population, and the older population has greater  
170 amplitude of oscillations and variance of chaotic dynamics than the younger population.

171 Our model is built on a number of simplifying assumptions. Risk tolerance and reactions  
172 to shifting prevalence are stratified by age class, but assumed homogeneous within each  
173 class. In reality, individuals would have heterogeneous risk tolerance according to their age,  
174 political affiliation, and other characteristics. We modeled adaptive behavior with dynamic  
175 within-group contact rates, but assumed between-group contact rates were fixed. While  
176 this was justified by COVID-19 public health policies that controlled within-group contact  
177 more than between-group contact, between-group contact is also responsive to prevalence.  
178 Further, we constrained the model with 4 mathematical assumptions (Eqs 2.10-2.13), some  
179 of which may not always hold in real-world scenarios. The relaxation of the above assump-  
180 tions may yield different model outcomes. However, while the thresholds between dynamical  
181 regimes may shift, the regimes themselves are likely robust. We note these assumptions were  
182 made in order to construct the simplest possible mathematical model that includes adaptive  
183 behavior and age-structured risk perceptions in an epidemic.

184 While the older population has a higher risk associated with infection, the younger popula-  
185 tion's lower aversion and higher baseline contact rates affect the epidemic dynamics in the  
186 older population. Thus, transmission in the young may not only lead to transmission in  
187 the elderly, but also increase the variance of the elderly dynamics and destabilize them. In  
188 Germany, youths were found to drive COVID-19 transmission dynamics in the first three  
189 pandemic waves [12]. Children are known to be the primary drivers of Influenza trans-  
190 mission, although severe morbidity and mortality are mostly seen in older age groups [39].  
191 The importance of the youth in the dynamics of our model provides theoretical support for  
192 COVID-19 lockdown policies that reduce between-group interaction (i.e.  $c_{ij}$ ), as found by  
193 Acemoglu et al. [15]. Transmission within the household is a key point of risk for the elderly  
194 and middle-aged, and high levels of transmission in the youth are likely to significantly affect  
195 disease outcomes in other age categories.

196 Our model may be usefully compared to other adaptive behavior models that look at sub-  
197 populations with differentiated characteristics or reactions to epidemic dynamics. It is worth  
198 noting that the justification for the bifurcated structure need not be restricted to age-based  
199 differentiation, but can also include political party affiliation, income levels, or other demo-  
200 graphic, social, behavioral, physical, or geographic differences. Some studies use structured  
201 2-population models with varying homophily and outgroup aversion or varying awareness  
202 separation and mixing separation [40, 41]. Results from these models indicate that het-  
203 erogeneous populations, even when simply structured compartmentally as two populations,  
204 can produce greater complexity in epidemic dynamics, including large second waves and



205 interconnected dual epidemics. Our results broadly agree with this theme: a 2-population  
206 model with varying infection aversion can produce more complexity at lower levels of trans-  
207 missibility, and the difference between aversions can also drive complexity (e.g Fig 5).

208 In our previous work [27], we compared the complex dynamics associated with endogenous  
209 behavior change during epidemics to similar theoretical behavior in ecological systems. Of-  
210 ten, when a single population is modeled in ecology (e.g. in a fishery [42]), the carrying  
211 capacity operates as an attractor, above which the population is attracted downwards and  
212 below which the population is attracted upwards. With endogenous behavior, the equilib-  
213 rium, or indifference point, is also an attractor, below which the population is motivated to  
214 relax protective behaviors and above which the population is motivated to adopt protective  
215 behaviors. It may be productive to extend this parallel further in the case of multiple pop-  
216 ulations. For example, the predator-prey model considers two interdependent populations.  
217 When the prey population is high, the predator population grows, but when the prey are  
218 low in number, the predators decrease. While our epidemiological model does not include  
219 such direct competition or predation, the behavior is somewhat similar: when the young  
220 population has high prevalence of disease, the prevalence in the older population increases  
221 until the indifference point is crossed. When the young population has low prevalence,  
222 the prevalence in the older population follows suit. If a comparison between ecology and  
223 epidemiology is appropriate, it follows that careful study of the literature in theoretical  
224 ecology may provide insights relevant to epidemiology, a field with as yet comparatively  
225 little exploration of such complex system dynamics.

226 We recommend further theoretical work in both adaptive behavior modeling and complexity  
227 in epidemiology. A systems perspective may better represent the inherent complexities  
228 and heterogeneities of real-world epidemics. Social drivers of disease have been relatively  
229 neglected in the literature [2], but played an important role in COVID-19 outcomes. For  
230 example, the divergence of risk assessment by age class that characterizes our model was a  
231 social phenomenon, though biologically motivated. Other complex phenomena important to  
232 COVID-19 include simultaneous asynchronous epidemics, political bifurcation of attitudes  
233 and practices, and the co-evolution of the human immune system and the virus. As public  
234 health policies depend on our ability to forecast different scenarios under a high degree of  
235 uncertainty and complexity, such modeling will play an important role in improving policy  
236 and health outcomes in future epidemics.

## References

- 237
- 238 [1] J. Bedson, L. A. Skrip, D. Pedi, S. Abramowitz, S. Carter, M. F. Jalloh, S. Funk,  
239 N. Gobat, T. Giles-Vernick, G. Chowell, J. R. de Almeida, R. Elessawi, S. V. Scarpino,  
240 R. A. Hammond, S. Briand, J. M. Epstein, L. Hébert-Dufresne, and B. M. Althouse,  
241 “A review and agenda for integrated disease models including social and behavioural  
242 factors,” *Nature Human Behaviour*, vol. 5, no. 7, pp. 834–846, 2021.
- 243 [2] R. F. Arthur, E. S. Gurley, H. Salje, L. S. P. Bloomfield, and J. H. Jones, “Contact  
244 structure, mobility, environmental impact and behavior: the importance of social forces  
245 to infectious disease dynamics and disease ecology,” *Philosophical Transactions of the  
246 Royal Society B*, vol. 372, p. 20160454, 2017.
- 247 [3] N. Ferguson, “Capturing Human behaviour,” *Nature*, vol. 446, no. April, p. 2007, 2007.
- 248 [4] J. Kerr, C. Panagopoulos, and S. van der Linden, “Political polarization on COVID-  
249 19 pandemic response in the United States,” *Personality and Individual Differences*,  
250 vol. 179, p. 110892, 2021.
- 251 [5] C. Latkin, L. A. Dayton, G. Yi, A. Konstantopoulos, J. Park, C. Maulsby, and X. Kong,  
252 “COVID-19 vaccine intentions in the United States, a social-ecological framework,”  
253 *Vaccine*, vol. 39, no. 16, pp. 2288–2294, 2021.
- 254 [6] C. Bonanad, S. García-Blas, F. Tarazona-Santabalbina, J. Sanchis, V. Bertomeu-  
255 González, L. Fácila, A. Ariza, J. Nunez, and A. Cordero, “The effect of age on mor-  
256 tality in patients with COVID-19: a meta-analysis with 611,583 subjects,” *Journal of  
257 the American Medical Directors Association*, vol. 21, no. 7, pp. 915–918, 2020.
- 258 [7] M. O’Driscoll, G. Ribeiro Dos Santos, L. Wang, D. A. T. Cummings, A. S. Azman,  
259 J. Paireau, A. Fontanet, S. Cauchemez, and H. Salje, “Age-specific mortality and  
260 immunity patterns of SARS-CoV-2,” *Nature*, vol. 590, no. 7844, pp. 140–145, 2021.
- 261 [8] M. K. Bundorf, J. DeMatteis, G. Miller, M. Polyakova, J. L. Streeter, and J. Wivagg,  
262 “Risk perceptions and protective behaviors: evidence from COVID-19 pandemic,” tech.  
263 rep., 2021.
- 264 [9] L. Korn, R. Siegers, S. Eitze, P. Sprengholz, F. Taubert, R. Böhm, and C. Betsch,  
265 “Age Differences in COVID-19 Preventive Behavior,” *European Psychologist*, 2022.
- 266 [10] S. Busenberg, K. Cooke, and M. Iannelli, “Endemic thresholds and stability in a class  
267 of age-structured epidemics,” *SIAM Journal on Applied Mathematics*, vol. 48, no. 6,  
268 pp. 1379–1395, 1988.

- 269 [11] H. Inaba, “Threshold and stability results for an age-structured epidemic model,” *Journal of mathematical biology*, vol. 28, no. 4, pp. 411–434, 1990.  
270
- 271 [12] I. Rodiah, P. Vanella, A. Kuhlmann, V. K. Jaeger, M. Harries, G. Krause, A. Karch,  
272 W. Bock, and B. Lange, “Age-specific contribution of contacts to transmission of sars-  
273 cov-2 in germany,” *European Journal of Epidemiology*, pp. 1–20, 2023.
- 274 [13] J. R. Goldstein, T. Cassidy, and K. W. Wachter, “Vaccinating the oldest against  
275 COVID-19 saves both the most lives and most years of life,” *Proceedings of the National*  
276 *Academy of Sciences*, vol. 118, no. 11, 2021.
- 277 [14] J. Dushoff, C. Colijn, D. J. D. Earn, and B. M. Bolker, “Transmission dynamics are  
278 crucial to COVID-19 vaccination policy,” *Proceedings of the National Academy of Sci-*  
279 *ences*, vol. 118, no. 29, p. e2105878118, 2021.
- 280 [15] D. Acemoglu, V. Chernozhukov, I. Werning, and M. D. Whinston, “Optimal targeted  
281 lockdowns in a multigroup SIR model,” *American Economic Review: Insights*, vol. 3,  
282 no. 4, pp. 487–502, 2021.
- 283 [16] E. P. Fenichel, C. Castillo-Chavez, M. G. Ceddia, G. Chowell, P. A. G. Parra, G. J.  
284 Hickling, G. Holloway, R. Horan, B. Morin, C. Perrings, M. Springborn, L. Velazquez,  
285 and C. Villalobos, “Adaptive human behavior in epidemiological models,” *Proceedings*  
286 *of the National Academy of Sciences*, vol. 108, no. 15, pp. 6306–6311, 2011.
- 287 [17] S. Funk, M. Salathé, and V. A. A. Jansen, “Modelling the influence of human behaviour  
288 on the spread of infectious diseases: a review,” *Journal of the Royal Society Interface*,  
289 vol. 7, no. 50, pp. 1247–1256, 2010.
- 290 [18] T. C. Reluga, “Game theory of social distancing in response to an epidemic,” *PLoS*  
291 *Computational Biology*, vol. 6, no. 5, pp. 1–9, 2010.
- 292 [19] J. M. Epstein, J. Parker, D. Cummings, and R. A. Hammond, “Coupled contagion  
293 dynamics of fear and disease: Mathematical and computational explorations,” *PLoS*  
294 *ONE*, vol. 3, no. 12, 2008.
- 295 [20] J. M. Epstein, E. Hatna, and J. Crodelle, “Triple contagion: A two-fears epidemic  
296 model,” *Journal of the Royal Society Interface*, vol. 18, no. 181, 2021.
- 297 [21] G. V. Bobashev and J. Epstein, “a Hybrid Epidemic Model: Combining the Advantages  
298 of Agent-Based and Equation-Based Approaches,” pp. 1532–1537, 2007.
- 299 [22] V. Capasso and G. Serio, “A generalization of the Kermack-McKendrick deterministic  
300 epidemic model,” *Mathematical Biosciences*, vol. 42, no. 1-2, pp. 43–61, 1978.

- 301 [23] W. K. A. McKendrick, “A Contribution to the Mathematical Theory of epidemics,”  
302 *Proceedings of the royal society of london. Series A, Containing papers of a mathemat-*  
303 *ical and physical character*, vol. 115, no. 772, pp. 700–721, 1927.
- 304 [24] T. Philipson, “Economic epidemiology and infectious diseases,” *Handbook of health*  
305 *economics*, vol. 1, pp. 1761–1799, 2000.
- 306 [25] A. D’Onofrio and P. Manfredi, “Information-related changes in contact patterns may  
307 trigger oscillations in the endemic prevalence of infectious diseases,” *Journal of Theo-*  
308 *retical Biology*, vol. 256, no. 3, pp. 473–478, 2009.
- 309 [26] A. Glaubitz and F. Fu, “Oscillatory dynamics in the dilemma of social distancing,”  
310 *Proceedings of the Royal Society A*, vol. 476, no. 2243, p. 20200686, 2020.
- 311 [27] R. F. Arthur, J. H. Jones, M. H. Bonds, Y. Ram, and M. W. Feldman, “Adaptive  
312 social contact rates induce complex dynamics during epidemics,” *PLoS Computational*  
313 *Biology*, vol. 17, no. 2, pp. 1–17, 2021.
- 314 [28] N. Sapkota, W. Karwowski, M. R. Davahli, A. Al-Juaid, R. Taiar, A. Murata, G. Wro-  
315 bel, and T. Marek, “The chaotic behavior of the spread of infection during the COVID-  
316 19 pandemic in the United States and globally,” *Ieee Access*, vol. 9, pp. 80692–80702,  
317 2021.
- 318 [29] A. Jones and N. Strigul, “Is spread of COVID-19 a chaotic epidemic?,” *Chaos, Solitons*  
319 *Fractals*, vol. 142, p. 110376, 2021.
- 320 [30] B. Bolker and B. T. Grenfell, “Space, persistence and dynamics of measles epidemics,”  
321 *Philosophical Transactions of the Royal Society of London. Series B: Biological Sci-*  
322 *ences*, vol. 348, no. 1325, pp. 309–320, 1995.
- 323 [31] B. T. Grenfell, “Chance and chaos in measles dynamics,” *Journal of the Royal Statis-*  
324 *tical Society: Series B (Methodological)*, vol. 54, no. 2, pp. 383–398, 1992.
- 325 [32] K. Dietz, “The incidence of infectious diseases under the influence of seasonal fluctua-  
326 tions,” in *Mathematical models in medicine*, pp. 1–15, Springer, 1976.
- 327 [33] J. L. Aron and I. B. Schwartz, “Seasonality and period-doubling bifurcations in an  
328 epidemic model,” *Journal of theoretical biology*, vol. 110, no. 4, pp. 665–679, 1984.
- 329 [34] W. M. Schaffer, “Can nonlinear dynamics elucidate mechanisms in ecology and epi-  
330 demiology?,” *IMA Journal of Mathematics Applied in Medicine and Biology*, vol. 2,  
331 no. 4, pp. 221–252, 1985.

- 332 [35] R. M. Anderson and R. M. May, “Vaccination against rubella and measles: quantitative  
333 investigations of different policies,” *Epidemiology Infection*, vol. 90, no. 2, pp. 259–325,  
334 1983.
- 335 [36] D. Schenzle, “An age-structured model of pre-and post-vaccination measles transmis-  
336 sion,” *Mathematical Medicine and Biology: A Journal of the IMA*, vol. 1, no. 2, pp. 169–  
337 191, 1984.
- 338 [37] W. O. Kermack and A. G. McKendrick, “A contribution to the mathematical theory  
339 of epidemics,” *Proceedings of the royal society of london. Series A, Containing papers  
340 of a mathematical and physical character*, vol. 115, no. 772, pp. 700–721, 1927.
- 341 [38] V. Ram and L. P. Schaposnik, “A modified age-structured SIR model for COVID-19  
342 type viruses,” *Scientific Reports*, vol. 11, no. 1, pp. 1–15, 2021.
- 343 [39] J. S. Brownstein, K. P. Kleinman, and K. D. Mandl, “Identifying pediatric age groups  
344 for influenza vaccination using a real-time regional surveillance system,” *American  
345 Journal of Epidemiology*, vol. 162, no. 7, pp. 686–693, 2005.
- 346 [40] P. E. Smaldino and J. H. Jones, “Coupled dynamics of behaviour and disease contagion  
347 among antagonistic groups,” *Evolutionary Human Sciences*, vol. 3, p. e28, 2021.
- 348 [41] M. J. Harris, K. J. Cardenas, and E. A. Mordecai, “Social divisions and risk perception  
349 drive divergent epidemics and large later waves,” *Evolutionary Human Sciences*, vol. 5,  
350 p. e8, 2023.
- 351 [42] W. E. Ricker, “Stock and recruitment,” *Journal of the Fisheries Board of Canada*,  
352 vol. 11, no. 5, pp. 559–623, 1954.